

Article

A New {Dy₅} Single-Molecule Magnet Bearing the Schiff Base Ligand *N*-Naphthalidene-2-amino-5-chlorophenol

Dimitris I. Alexandropoulos ¹, Alysha A. Alaimo ¹, Di Sun ²  and Theocharis C. Stamatatos ^{1,*} 

¹ Department of Chemistry, 1812 Sir Isaac Brock Way, Brock University, St. Catharines, ON L2S 3A1, Canada; da12he@icloud.com (D.I.A.); aa08mi@brocku.ca (A.A.A.)

² Key Lab of Colloid and Interface Chemistry, Ministry of Education, School of Chemistry and Chemical Engineering, Shandong University, Jinan 250100, China; dsun@sdu.edu.cn

* Correspondence: tstatamatatos@brocku.ca; Tel.: +1-905-688-5560 (ext. 3400)

Received: 1 October 2018; Accepted: 25 October 2018; Published: 1 November 2018



Abstract: A new {Dy₅} cluster compound has been synthesized and structurally characterized from the initial use of the Schiff base ligand *N*-naphthalidene-2-amino-5-chlorophenol (nacpH₂) in coordination chemistry. The 1:1 reaction between Dy(hpd)₃·2H₂O and nacpH₂, in a solvent mixture comprising CH₂Cl₂ and MeOH, afforded orange crystals of [Dy₅(OH)₂(hpd)₃(nacp)₅(MeOH)₅] (**1**) in 70% yield, where hpd[−] is the anion of 3,5-heptadione. The {Dy₅} complex can be described as two vertical {Dy₃(μ₃-OH)}⁸⁺ triangles sharing a common vertex; such a metal topology is unprecedented in 4*f*-metal cluster chemistry. Direct current (dc) magnetic susceptibility studies revealed the presence of some weak ferromagnetic exchange interactions between the five Dy^{III} ions at low temperatures. Alternating current (ac) magnetic susceptibility measurements at zero applied dc field showed that complex **1**·3MeOH·CH₂Cl₂ exhibits temperature- and frequency-dependent out-of-phase signals below ~20 K, characteristics of a single-molecule magnet (SMM). The resulting relaxation times were used to construct an Arrhenius-type plot and determine an effective energy barrier, *U*_{eff}, of 100 K for the magnetization reversal. The application of a small dc field of 200 Oe resulted in the surpassing of the quantum tunneling process and subsequently the increase of the *U*_{eff} to a value of 170 K. The reported results are part of a long-term program aiming at the preparation of structurally and magnetically interesting lanthanide complexes bearing various Schiff base chelating/bridging ligands.

Keywords: dysprosium; schiff bases; cluster compounds; single-molecule magnets; crystal structures

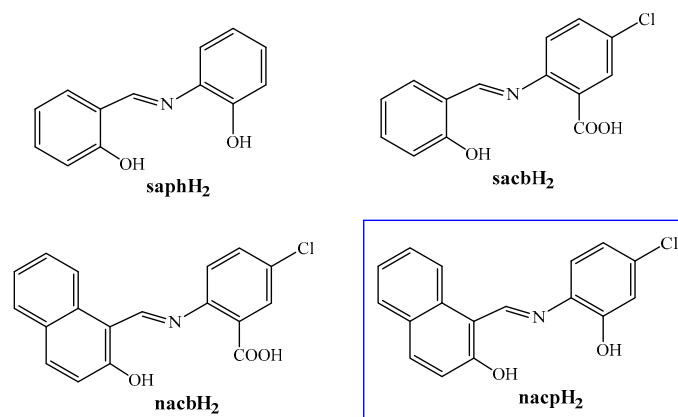
1. Introduction

The coordination chemistry of 4*f*-metal ions has recently re-attracted the interest of the scientific community for three primary reasons: (i) their ability to form oligo- and polynuclear metal complexes (clusters) with unprecedented and nanosized structures [1], (ii) the unusual photoluminescence properties they exhibit [2], arising from forbidden 4*f*-4*f* electronic transitions that emerge when coordinated organic ligands are involved, and (iii) their pivotal role in the development of efficient single-molecule magnets (SMMs) [3]. SMMs are individual molecular compounds that exhibit slow relaxation of their magnetization in the absence of an external magnetic field [4]. Such a magnetization reversal is accomplished by the presence of an anisotropic energy barrier, *U*, which operates through various mechanisms that are either spin-lattice processes (Raman, Orbach and direct mechanism) or quantum tunneling of magnetization (QTM) [5]. Due to their molecular properties (i.e., solubility, crystallinity, etc.), SMMs have been proposed as promising candidates for various modern technological advancements, such as in information and data storage, molecular spintronics and quantum computing [6].

In the case of $4f$ -metal ions, the energy barrier U (or, more explicitly, the effective energy barrier, U_{eff}) arises from the spin-orbit coupled electronic ground states ($^{2S+1}L_J$) which can be further split into $\pm m_J$ microstates in the presence of an appropriate crystal field [7]. Therefore, the crystal field has a pronounced effect on the resulting magnetization dynamics. Subsequently, the choice of the coordinated ligands becomes an obvious synthetic challenge. In addition to the bistable ground state, another requirement for a $4f$ -SMM is the large total angular momentum (J). This is also assisted by the ligand-field around the metal ion(s), which can stabilize the largest projection of the total angular momentum. Based on these prerequisites, it becomes apparent why Dy^{III} ($^6\text{H}_{15/2}$) is a key element to the synthesis of SMMs with interesting properties. The non-integer value of J in Dy^{III} ions results in a Kramers doublet ground state, i.e., a degenerate pair of $\pm m_J$ microstates, which produces a bistable magnetic moment that can be used to store information at a molecular level. Thus, the optimization of the lanthanide's coordination environment towards highly-symmetric polyhedra and ideal geometries has become a *sine qua non* in the field of SMMs [8]. It was theoretically predicted and practically proven that high-symmetry coordination geometries render possible the control of the fast QTM through the disappearance of certain terms in the crystal field Hamiltonian [9].

To gain access into some of these exciting properties, the synthesis of new Dy^{III} complexes is apparently necessary for both the development of structure-magnetism relationships and the elaboration of key factors that affect the chemical and magnetic dynamics of a molecular compound. To this end, we have recently started a program aimed at the employment of various Schiff base ligands (Scheme 1) in Dy^{III} chemistry as a means of obtaining structurally new and magnetically interesting complexes. Indeed, the use of *N*-salicylidene-*o*-aminophenol (saphH₂) in Dy^{III} chemistry has resulted in the formation of a {Dy₇} SMM exhibiting a very small energy barrier of ~4 K for the magnetization reversal [10]. Our next synthetic attempts were oriented towards the synthesis of Dy^{III} /sacbH₂ complexes, where sacbH₂ is the Schiff base ligand *N*-salicylidene-2-amino-5-chlorobenzoic acid; a new {Dy₂} SMM was prepared and it exhibited a large energy barrier of ~109 K [11]. The reasonable next step to follow was the exploration of the coordination capabilities of *N*-naphthalidene-2-amino-5-chlorobenzoic acid (nacbH₂), which is similar to sacbH₂ but with an additional aromatic ring on the *N*-salicylidene moiety. Although we have been successful with the synthesis of many $3d$ -metal complexes [12], we have been unable to date to isolate any $4f$ -metal compound bearing the ligand nacbH₂.

The last member of this tetralogy of Schiff base ligands was *N*-naphthalidene-2-amino-5-chlorophenol (nacpH₂), in structural, electronic and chemical analogy to saphH₂ (and in part to nacbH₂). We here report the detailed synthesis and characterization of the ligand nacpH₂, and its first use in coordination chemistry that allowed us to isolate and study a new {Dy₅} cluster compound with a bent bowtie topology, and SMM behavior with a large energy barrier of 100 K.

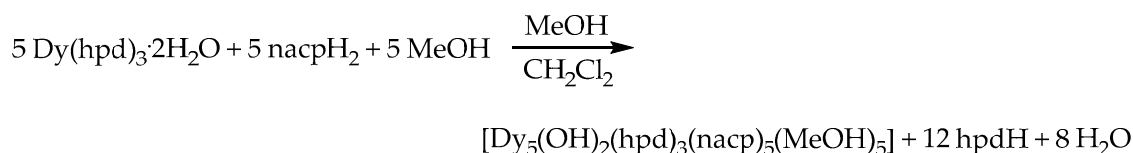


Scheme 1. Structural formulas and abbreviations of the Schiff base ligands discussed in the text; the blue box encloses the tridentate ligand nacpH₂ used in the present work.

2. Results and Discussion

2.1. Synthetic Comments

Many synthetic routes to oligo- and polynuclear 4*f*-metal complexes rely on the employment of β -diketones either alone or in conjunction with various chelating/bridging ligands [13,14]. This is clearly because β -diketonate groups are excellent capping, and occasionally bridging ligands, thus fulfilling the coordination needs of the lanthanide ions. Furthermore, they are O-donor ligands which can satisfy the oxophilicity of the Ln^{III} ions and form stable five-membered chelate rings that enhance the stability of the resulting compounds. Lastly, β -diketonate ions are also known for their ability to act as Lewis bases and consequently abstract the H-atoms from the OH-groups of the corresponding organic chelating/bridging ligands, such as nacpH₂ in the present case. Among all the available β -diketones, only 3,5-heptadione was able to facilitate the formation of a crystalline product in this work. Therefore, the reaction between Dy(hpd)₃·2H₂O and nacpH₂ in a 1:1 molar ratio, in a solvent mixture comprising CH₂Cl₂ and MeOH, afforded orange crystals of a new [Dy₅(OH)₂(hpd)₃(nacp)₅(MeOH)₅] (**1**) cluster in yields as high as 70%. The general formation of **1** is summarized by Scheme 2.



Scheme 2. General formation of complex **1**.

Complex **1** is very stable under the reported conditions, and its identity is not dependent on either the presence of an external base (i.e., NEt₃, NMe₃, NPr₃, and Me₄NOH) or the molar ratio of the reagents. However, its crystallinity and yields are largely affected by the appropriate solvent mixture (CH₂Cl₂/MeOH). More specifically, the same reaction in only CH₂Cl₂ or MeOH gave amorphous solids or microcrystalline materials, respectively, which we were either unable to further characterize (in the case of CH₂Cl₂ only) or able to identify as the {Dy₅} compound based on IR spectroscopic studies and elemental analyses (in the case of MeOH only). Furthermore, analogous reactions but in 2:1 and 1:2 Dy(hpd)₃·2H₂O:nacpH₂ molar ratios gave crystals of **1** in very low yield (i.e., 5–15%).

2.2. Description of Structure

A partially labelled structure of complex **1** is shown in Figure 1. The molecular compound crystallizes with three MeOH and one CH₂Cl₂ solvate molecules, which appear in the crystal lattice of **1**. A view of the core of **1** and its metallic skeleton are illustrated in Figure 2 (top and bottom, respectively). Selected interatomic distances and angles are listed in Table S1. The crystallographically established coordination modes of the ligands hpd[−] and nacp^{2−} present in complex **1** are shown in Figure S1.

The molecular structure of **1** (Figure 1) consists of five Dy^{III} ions held together by two μ_3 -bridging OH[−] ions (O13 and O26), one bidentate chelating/bridging hpd[−] group (acting as an $\eta^1\text{-}\eta^2\text{:}\mu$ ligand), and the naphthoxido and phenoxido arms of three $\eta^1\text{:}\eta^1\text{:}\eta^2\text{:}\mu$ and two $\eta^2\text{:}\eta^1\text{:}\eta^2\text{:}\mu_3$ nacp^{2−} ligands (Figure S1). Peripheral ligation about the complete [Dy₅(μ_3 -OH)₂(μ -OR)₈]⁵⁺ core (Figure 2, top) is provided by the chelating parts of the nacp^{2−} ligands, two bidentate chelating hpd[−] groups (on Dy2 and Dy3), and five terminal MeOH molecules (on Dy1, Dy2 and Dy4). The overall metal topology of **1** can be described as two nearly isosceles {Dy₃(μ_3 -OH)}⁸⁺ triangles (Table S1), which are vertical to each other and they share a common Dy₅ vertex (a bowtie topology; Figure 2, bottom). The angle between the two triangular planes is 89.7°. The OH[−] groups are displaced 0.919 Å (O13) and 0.894 Å (O26) out of the Dy₃⋯Dy₄⋯Dy₅ and Dy₁⋯Dy₂⋯Dy₅ planes, respectively. There are very few reported {Dy₅} clusters with a bowtie topology in the literature [15–18] and complex **1** is the first of its type with

such a distorted, bent arrangement. Moreover, to our knowledge, complex **1** is the first structurally characterized complex bearing the anion of hpd^- as a coordinated ligand. Finally, the structure of **1** is stabilized by several strong intramolecular H-bonds that involve the hydroxido, phenoxido (from nac^{2-}) and MeOH groups (both coordinated and lattice). In addition, the lattice CH_2Cl_2 molecules appear to occupy the voids created by the supramolecular arrangement of the $\{\text{Dy}_5\}$ clusters.

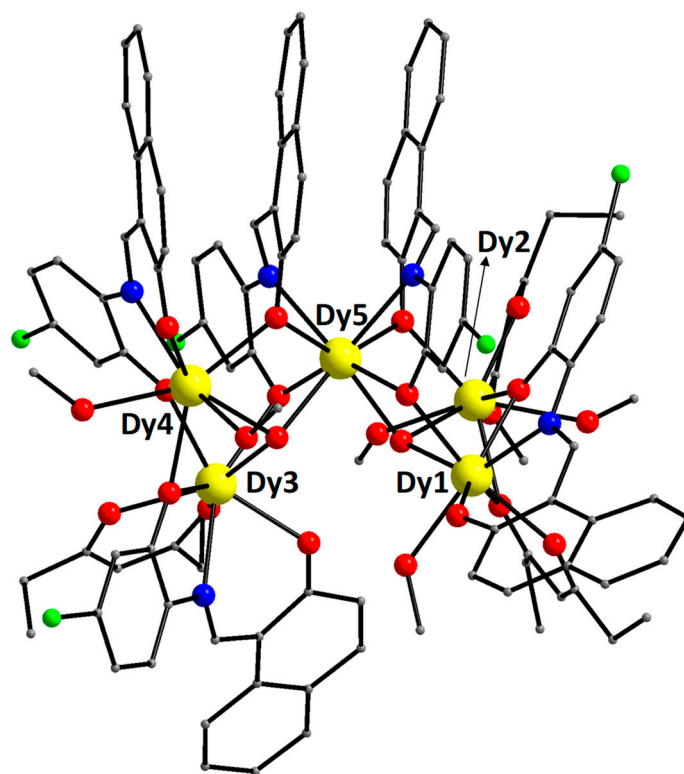


Figure 1. Partially labeled representation of the molecular structure of **1**. Color scheme: Dy^{III} , yellow; Cl, purple; O, red; N, green; C, gray. H atoms are omitted for clarity.

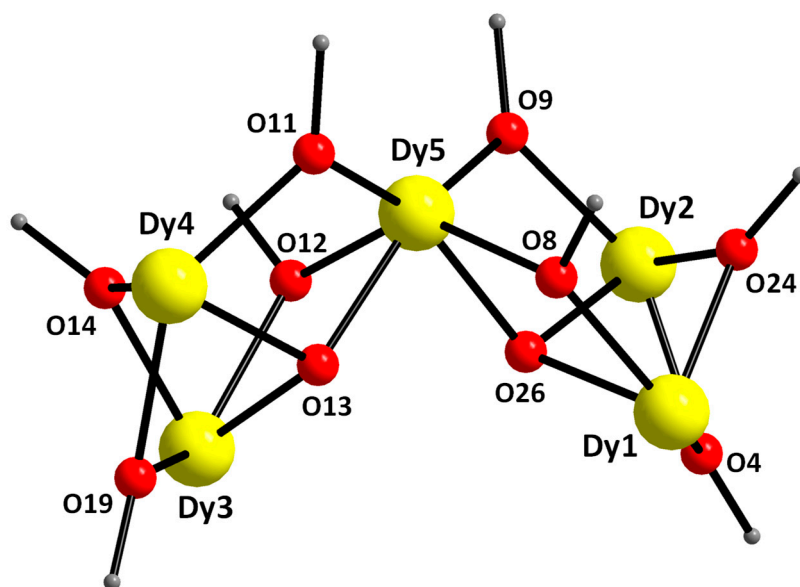


Figure 2. *Cont.*

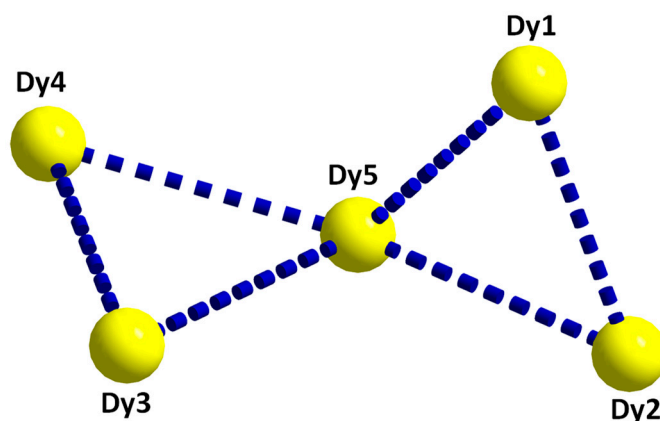


Figure 2. (Top) The complete $[\text{Dy}_5(\mu_3\text{-OH})_2(\mu\text{-OR})_8]^{5+}$ core of **1**, and (bottom) its $\{\text{Dy}_5\}$ bowtie-like topology. The blue dashed lines are virtual bonds to show the two vertex-sharing triangles. Color scheme as in Figure 1.

All Dy^{III} ions are eight-coordinate albeit with different geometries. The coordination geometries were determined by the continuous shape measures (CShM) approach of the SHAPE program [19], which allows one to numerically evaluate by how much a particular polyhedron deviates from the ideal shape. The best fits were obtained for the square antiprismatic (CShM values = 1.53 and 1.10 for Dy3 and Dy5, respectively), triangular dodecahedral (CShM values = 1.40 and 1.03 for Dy1 and Dy4, respectively), and biaugmented trigonal prismatic (CShM value = 1.52 for Dy2) geometries (Figure 3, Table S2). Values of CShM between 0.1 and 3 usually correspond to a not negligible, but still small distortion from ideal geometry [20].

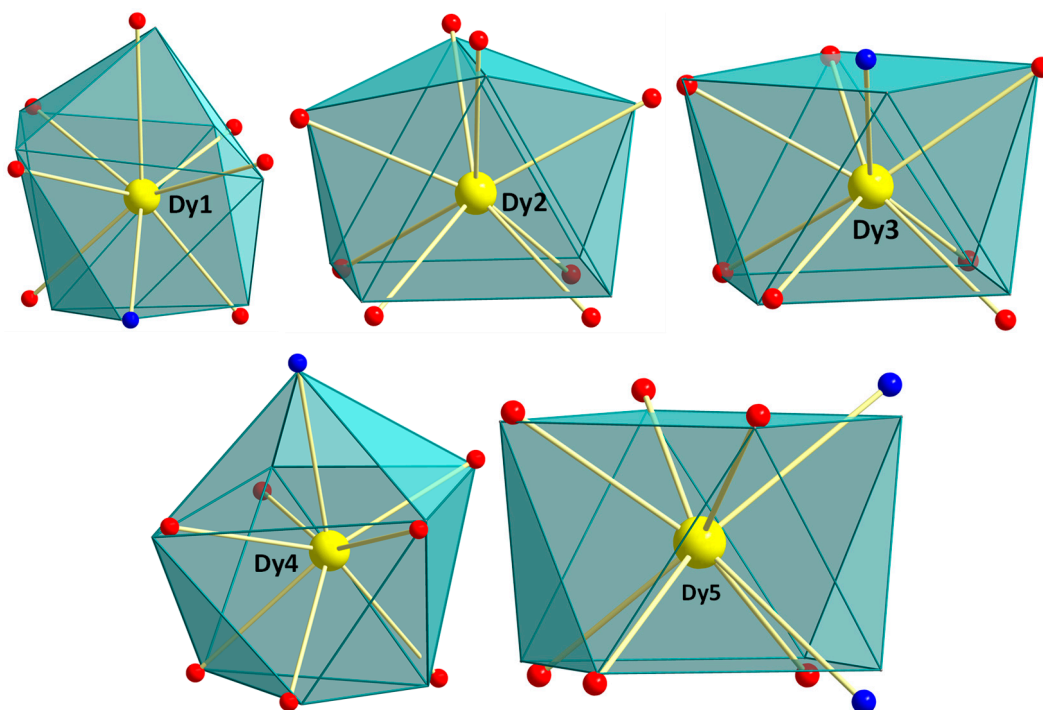


Figure 3. Square antiprismatic, triangular dodecahedral and biaugmented trigonal prismatic coordination geometries of the Dy atoms in **1**. Points connected by the gray thin lines define the vertices of the ideal polyhedra.

2.3. Solid-State Magnetic Susceptibility Studies

Direct current (dc) magnetic susceptibility measurements on a crystalline sample of complex $1 \cdot 3\text{MeOH} \cdot \text{CH}_2\text{Cl}_2$ were performed in the 2–300 K range under an applied magnetic field of 0.1 T (Figure 4). The room-temperature $\chi_M T$ value of $70.48 \text{ cm}^3 \text{Kmol}^{-1}$ is very close to the theoretical value of $70.85 \text{ cm}^3 \text{Kmol}^{-1}$ for five non-interacting Dy^{III} ions (${}^6\text{H}_{15/2}$, $S = 5/2$, $L = 5$, $g = 4/3$). The $\chi_M T$ product declines gradually on cooling until ~ 20 K, it then plateaus at a value of $\sim 63 \text{ cm}^3 \text{Kmol}^{-1}$ from 20 to 10 K, and it finally increases to reach a value of $64.78 \text{ cm}^3 \text{Kmol}^{-1}$ at 2.5 K. The decrease of the $\chi_M T$ product in the 300–20 K region is mainly due to the depopulation of the crystal field (CF) m_j states, whereas the low-temperature incline may be attributed to some weak intramolecular ferromagnetic exchange interactions between the Dy^{III} ions. The drop of the $\chi_M T$ product below 2.5 K could be assigned to effects from the magnetic anisotropy, the presence of intermolecular interactions and the applied dc field (Zeeman effect). The field dependence of the magnetization at 1.9, 3 and 5 K shows a relatively fast increase at low fields without reaching saturation at 7 T, which presages significant magnetic anisotropy (Figure 4, inset). Furthermore, the magnetization value at 7 T is $\sim 30 N\mu_B$, much lower than the expected value for five Dy^{III} ions ($M_S/N\mu_B = n g J = 50 N\mu_B$), which is due to the CF effects that induce strong magnetic anisotropy.

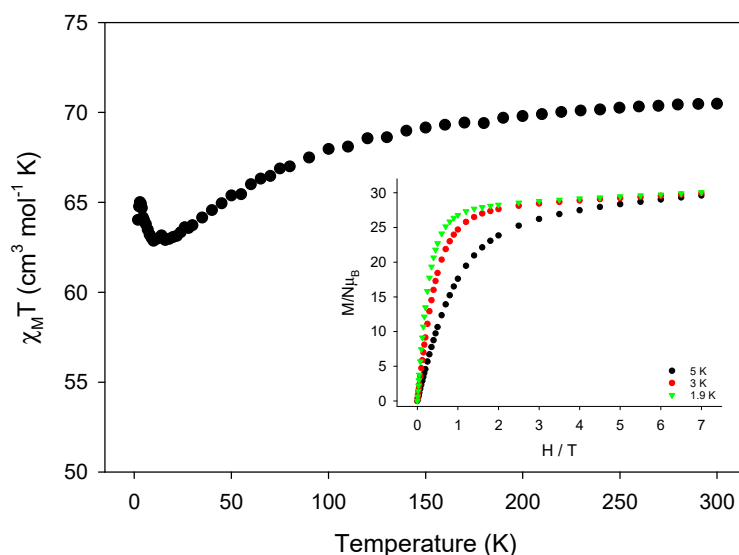


Figure 4. Temperature dependence of the $\chi_M T$ product for complex $1 \cdot 3\text{MeOH} \cdot \text{CH}_2\text{Cl}_2$ at 0.1 T. (inset) Plots of magnetization (M) versus field (H) for complex $1 \cdot 3\text{MeOH} \cdot \text{CH}_2\text{Cl}_2$ at three different low temperatures.

To probe the magnetic dynamics of $1 \cdot 3\text{MeOH} \cdot \text{CH}_2\text{Cl}_2$, alternating current (ac) magnetic susceptibility measurements, as a function of both temperature (Figure 5) and frequency (Figure 6), were initially performed in zero applied dc field. The compound displays frequency-dependent tails of signals in the χ_M' (in-phase susceptibility) and χ_M'' (out-of-phase susceptibility) versus T plots at temperatures below ~ 15 K, suggesting the presence of slow relaxation of the magnetization consistent with an SMM behavior. The tails of signals are suggestive of the presence of fast quantum tunneling of magnetization (QTM), without precluding though the concurrent presence of thermally-assisted processes. To this end, we studied the dependence of the χ_M' and χ_M'' susceptibilities on the ac frequency at each temperature (1.9–13 K, Figure 6).

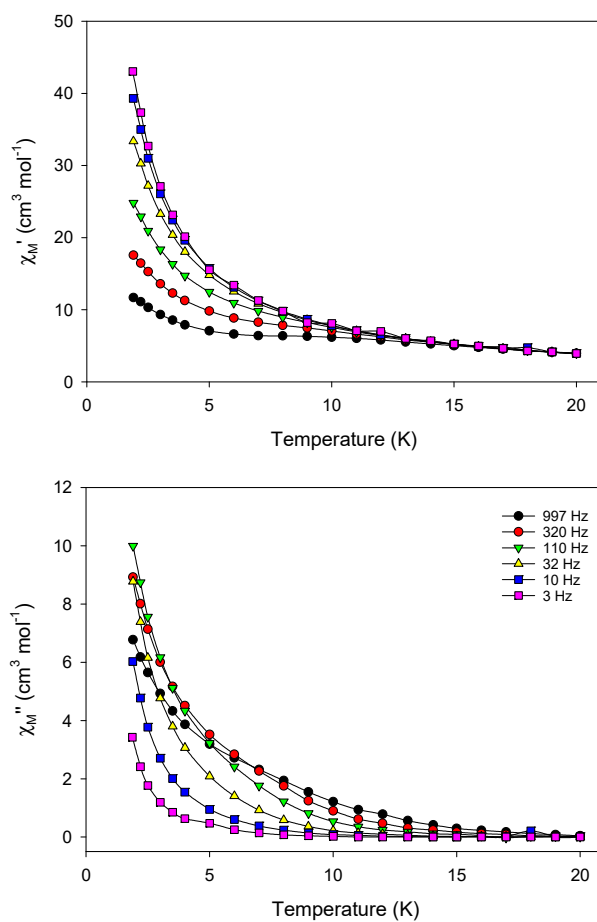


Figure 5. Temperature dependence of the in-phase (χ_M' , **top**) and out-of-phase (χ_M'' , **bottom**) ac magnetic susceptibilities at zero dc field for 1·3MeOH·CH₂Cl₂, measured in a 3.0 G ac field oscillating at the indicated frequencies. The solid lines are guides only.

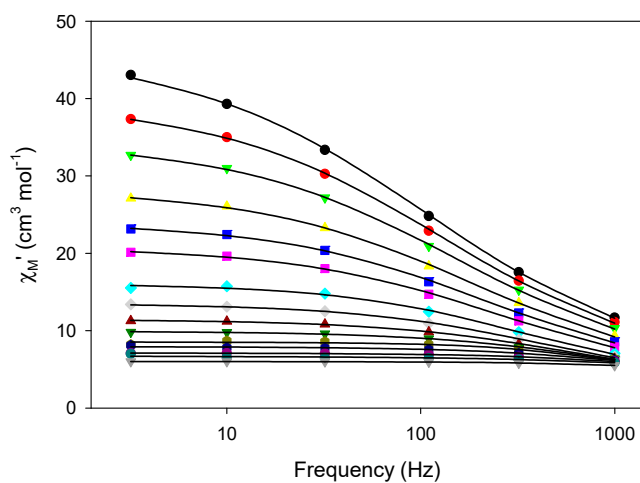


Figure 6. *Cont.*

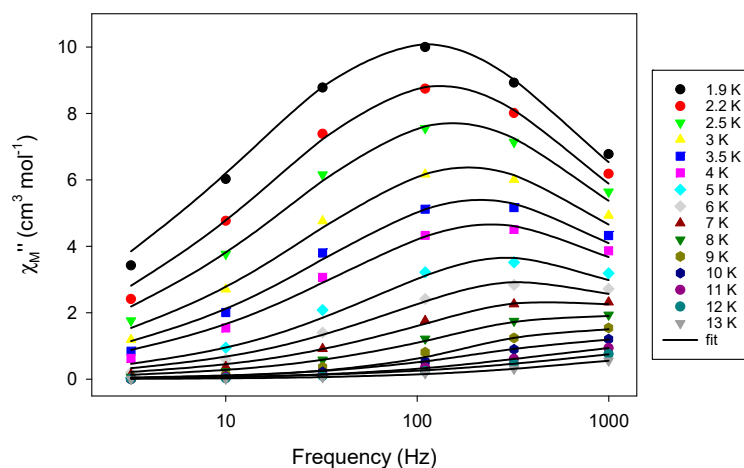


Figure 6. Frequency dependence of the in-phase (χ_M' , **top**) and out-of-phase (χ_M'' , **bottom**) ac magnetic susceptibilities at zero dc field for $1 \cdot 3\text{MeOH} \cdot \text{CH}_2\text{Cl}_2$, measured in a 3.0 G ac field at the temperature range 1.9–13 K. Solid lines represent fits to the data, as described in the main text.

The peak maxima allowed us to fit the data to a generalized Debye function [21] and extract the temperature-dependent relaxation times (τ), which subsequently allowed us to assess the operative magnetic relaxation for an SMM. In an ideal case, when an activation barrier exists with respect to the magnetization reversal, the system must exchange energy with the lattice (in the form of phonons) to ascend to the top of the barrier before relaxation can take place [22]. Such a relaxation process, known as the Orbach mechanism, results in an exponential dependence of τ upon temperature. Consequently, an Arrhenius-type plot can be constructed and from this the effective energy barrier, U_{eff} , and pre-exponential factor, τ_0 , can be derived. As shown in Figure 7 (left), the plot of $\ln\tau$ versus $1/T$ exhibits a linear shape at high temperatures, corresponding to a thermally-activated Orbach process. The curvature of the plot at lower temperatures suggests that additional relaxation processes are still operative. Therefore, we fitted the $\ln\tau$ versus $1/T$ data of $1 \cdot 3\text{MeOH} \cdot \text{CH}_2\text{Cl}_2$ using Equation (1), which accounts for the presence of QTM (first term), Raman (second term) and Orbach (last term) relaxation processes over the entire temperature range. A very good fit of the data was obtained with the following best-fit parameters: $U_{\text{eff}} = 100(1)$ K, $\tau_0 = 1.0(1) \times 10^{-7}$ s, $n = 6.90$, $C = 5.0 \times 10^{-4} \text{ s}^{-1}\text{K}^{-n}$ and $\tau_{\text{QTM}} = 0.10$ s.

$$\tau_{\text{obs}}^{-1} = \tau_{\text{QTM}}^{-1} + CT^n + \tau_0^{-1} \exp(-U_{\text{eff}}/kT) \quad (1)$$

The deviation of the lower-temperature relaxation data from linearity is due to the interplay between QTM and thermally assisted relaxation processes. This is a usual phenomenon in cluster compounds of Kramers ions at different coordination geometries [23]. It is very likely that the presence of easy-axis anisotropy, dipole-dipole and hyperfine interactions in **1** allow the mixing of the ground states of the five Kramers ions, thus promoting the QTM over a thermally-assisted pathway [24,25]. In fact, the Cole-Cole plots (Figure S6, top) for $1 \cdot 3\text{MeOH} \cdot \text{CH}_2\text{Cl}_2$ in the temperature range 1.9–13 K exhibit semicircular shapes and the data were fit by using a generalized Debye model. The α values were in the range 0.44–0.17, suggesting the presence of multiple relaxation processes [26].

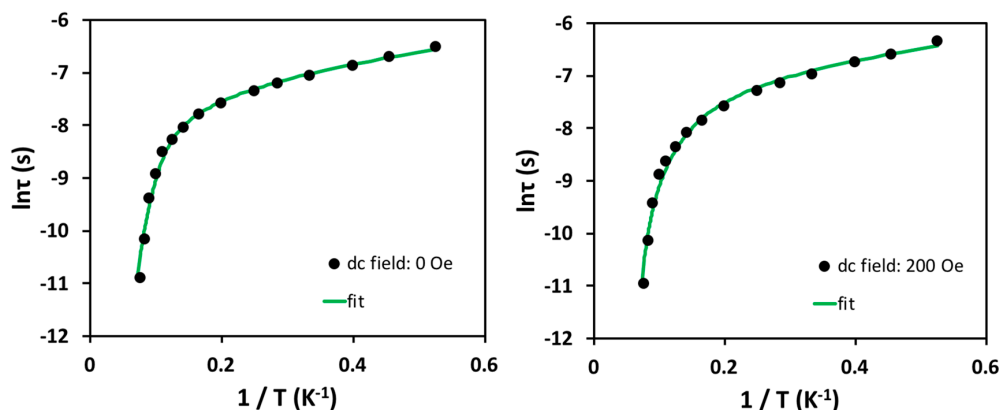


Figure 7. Arrhenius plots of 1:3MeOH·CH₂Cl₂ at zero (left) and 200 Oe (right) applied dc fields. The green lines correspond to the fit of the data; see the text for the fit parameters.

To further study the magnetic dynamics of 1:3MeOH·CH₂Cl₂ and attempt to suppress the effective QTM, ac measurements were also carried out under an applied, optimum dc field of 200 Oe (Figure S2). The peak maxima in the χ_M'' versus frequency plot (Figure 8) allowed us to fit the data to a generalized Debye model and the extracted relaxation times were then used to construct the Arrhenius-type plot (Figure 7, right), from which we derived the following fitting parameters (using Equation (1)): $U_{\text{eff}} = 170(1)$ K, $\tau_0 = 1.6(1) \times 10^{-9}$ s, $n = 4.74$, $C = 0.10 \text{ s}^{-1}\text{K}^{-n}$ and $\tau_{\text{QTM}} = 0.01$ s. The obtained parameters agree well with an elimination of the QTM and consequently an increase of the U_{eff} barrier. The Cole-Cole plots (Figure S6, bottom) for 1:3MeOH·CH₂Cl₂ in the temperature range 1.9–15 K (under 200 Oe field) exhibit again semicircular shapes; the data were fit and the corresponding α values were in the range 0.46–0.05. Finally, it is worthy to note that among the {Dy₅} clusters with a bowtie topology [15–18], complex 1 is the only one exhibiting ferromagnetic exchange interactions between the metal centers and it has the second largest energy barrier for the magnetization reversal. Tang, Li and coworkers reported an asymmetric {Dy₅} bowtie cluster exhibiting SMM behavior with a barrier of 197 K; the Dy^{III} atoms were 8- and 9-coordinate and antiferromagnetic exchange interactions were observed [15]. All the remaining {Dy₅} complexes with a bowtie metal topology possess various Dy^{III} coordination geometries and weak SMM properties. It is difficult to conclude at this stage of research which factor contributes mostly to the enhancement of the SMM properties within the reported {Dy₅} complexes with a bowtie metal arrangement. It is very likely that the combination of the appropriate Dy^{III} coordination geometries, the distortion of the {Dy₅} core, and the nature of the predominant magnetic exchange interactions play a vital role on the onset of the magnetization dynamics.

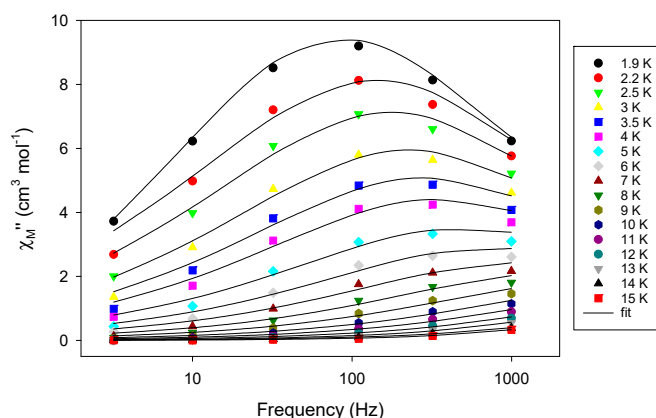


Figure 8. Frequency dependence of the out-of-phase (χ_M'') ac magnetic susceptibility at 200 Oe dc field for 1:3MeOH·CH₂Cl₂, measured in a 3.0 G ac field at the temperature range 1.9–15 K. Solid lines represent fits to the data, as described in the main text.

3. Experimental Section

3.1. Materials, Physical and Spectroscopic Measurements

All manipulations were performed under aerobic conditions using materials (reagent grade) and solvents as received unless otherwise noted. The precursor $\text{Dy}(\text{hpd})_3 \cdot 2\text{H}_2\text{O}$ ($\text{hpd}^- = 3,5\text{-heptadione anion}$) was synthesized following previously reported methods for various lanthanide(III) β -diketonate starting materials [27]. The Schiff base ligand *N*-naphthalidene-2-amino-5-chlorophenol (nacpH_2) was prepared in a manner similar to that of *N*-naphthalidene-2-amino-5-chlorobenzoic acid (nacbH_2) [12]. Infrared spectra were recorded in the solid state on a Bruker's FT-IR spectrometer (ALPHA's Platinum ATR single reflection) in the $4000\text{--}400\text{ cm}^{-1}$ range. Elemental analyses (C, H, and N) were performed on a Perkin-Elmer 2400 Series II Analyzer. Melting points were measured on an Electrothermal Apparatus-9100. Electrospray ionization (ESI) mass spectra (MS) of nacpH_2 in MeCN were taken on a Bruker HCT Ultra mass spectrometer. NMR spectra were obtained on a Bruker Avance DPX-400 MHz instrument and are referenced to the residual proton signal of the deuterated solvent for ^1H and ^{13}C spectra according to published values. Variable-temperature direct and alternating current (dc and ac, respectively) magnetic susceptibility studies were conducted at the temperature range 1.9–300 K using a Quantum Design MPMS XL-7 SQUID magnetometer equipped with a 7 T magnet. Pascal's constants were used to estimate the diamagnetic correction [28], which was subtracted from the experimental susceptibility to give the molar paramagnetic susceptibility (χ_M).

3.2. Synthesis of nacpH_2

The organic ligand *N*-naphthalidene-2-amino-5-chlorophenol (nacpH_2) was prepared in quantitative yields (~95%) by the condensation reaction of 2-amino-5-chlorophenol (7.18 g, 50 mmol) with 2-hydroxy-1-naphthaldehyde (8.61 g, 50 mmol) in a molar ratio of 1:1 in 100 mL of refluxing MeOH. The reaction was stirred under reflux for 3 h and then cooled down to room temperature, during which time a brown microcrystalline solid had appeared. The brown solid was collected by filtration, dried under vacuum, and analyzed as solvent-free. Anal. calc. for $\text{C}_{17}\text{H}_{12}\text{NO}_2\text{Cl}$ (found values in parentheses): C 68.58 (68.71), H 4.06 (4.12), N 4.70 (4.55) %. M.p.: 184–186 °C. Selected IR data (ATR): $\nu = 1615$ (vs), 1587 (m), 1542 (s), 1508 (m), 1481 (m), 1427 (m), 1403 (m), 1347 (s), 1305 (m), 1263 (m), 1208 (m), 1185 (m), 1156 (m), 1138 (s), 1089 (m), 1040 (m), 983 (m), 967 (m), 941 (m), 903 (m), 879 (m), 861 (s), 828 (m), 793 (m), 746 (m), 721 (s), 684 (vs), 628 (m), 525 (m), 481 (vs), 463 (s), 444 (s), 434 (m). ^1H NMR (DMSO- d_6 , ppm; Figure S3): δ 15.70 (s, 1H; -OH), 10.79 (s, 1H; -OH), 9.53 (s, 1H; -CH=N), 6.82–8.42 (m, 9H, 9-Ar-H). ^{13}C NMR (DMSO- d_6 , ppm; Figure S4): δ 176.3, 150.4, 149.5, 137.9, 133.7, 130.1, 120.0, 128.6, 128.1, 126.0, 124.5, 123.2, 120.0, 119.6, 119.1, 115.6, 108.1. Positive ESI-MS (m/z ; Figure S5): 298 (M-H $^+$).

3.3. Synthesis of $[\text{Dy}_5(\text{OH})_2(\text{hpd})_3(\text{nacp})_5(\text{MeOH})_5]$ (1)

To a stirred, brown suspension of nacpH_2 (0.06 g, 0.20 mmol) in CH_2Cl_2 (10 mL) was added a yellowish solution of $\text{Dy}(\text{hpd})_3 \cdot 2\text{H}_2\text{O}$ (0.14 g, 0.20 mmol) in MeOH (20 mL). The resulting dark orange solution was stirred for 20 min, filtered and the filtrate was left to evaporate slowly at room temperature. After three days, X-ray quality orange plate-like crystals of $1 \cdot 3\text{MeOH} \cdot \text{CH}_2\text{Cl}_2$ were formed and these were collected by filtration, washed with cold MeOH ($2 \times 3\text{ mL}$), and dried in air. The yield was 70% (based on the ligand available). The air-dried solid was satisfactorily analyzed as lattice-solvent free, i.e., as 1. Anal. calc. for $\text{C}_{111}\text{H}_{105}\text{N}_5\text{O}_{23}\text{Dy}_5\text{Cl}_5$ (found values in parentheses): C 46.51 (46.77), H 3.69 (3.74), N 2.44 (2.12) %. Selected IR data (ATR): $\nu = 1617$ (vs), 1578 (s), 1509 (s), 1475 (m), 1456 (m), 1386 (m), 1334 (m), 1290 (m), 1262 (m), 1174 (m), 1154 (m), 1121 (m), 1069 (m), 1018 (m), 980 (m), 947 (m), 912 (vs), 881 (m), 854 (m), 829 (m), 776 (m), 743 (s), 676 (m), 619 (s), 597 (m), 536 (mb), 501 (m), 464 (vs), 416 (m), 407 (m).

3.4. Single-Crystal X-ray Crystallography

Single-crystal X-ray diffraction data were collected on an orange plate-like crystal ($0.05 \times 0.04 \times 0.02$ mm) of complex $1 \cdot 3\text{MeOH} \cdot \text{CH}_2\text{Cl}_2$ using a Rigaku Oxford Diffraction XtaLAB Synergy diffractometer equipped with a HyPix-6000HE area detector at 100 K and utilizing Mo $K\alpha$ ($\lambda = 0.71073 \text{ \AA}$) from PhotonJet micro-focus X-ray source. The structure was solved using the charge-flipping algorithm, as implemented in the program SUPERFLIP [29], and refined by full-matrix least-squares techniques against F_o^2 using the SHELXL program [30] through the OLEX2 interface [31]. The non-hydrogen atoms were successfully refined using anisotropic displacement parameters, and hydrogen atoms bonded to the carbon of the ligands and those of the hydroxido groups were placed at their idealized positions using appropriate *HFIX* instructions in SHELXL. All these atoms were included in subsequent refinement cycles in riding-motion approximation with isotropic thermal displacement parameters (U_{iso}) fixed at 1.2 or $1.5 \times U_{\text{eq}}$ of the relative atom. Various figures of the structure were created using the Diamond 3 program package [32]. Unit cell parameters, structure solution and refinement details for $1 \cdot 3\text{MeOH} \cdot \text{CH}_2\text{Cl}_2$ are summarized in Table S3. Further crystallographic details can be found in the corresponding CIF file provided in the ESI.

Crystallographic data for the structure of **1** have been deposited with the Cambridge Crystallographic Data Centre (CCDC) as supplementary publication number: CCDC-1868805. Copies of these data can be obtained free of charge on application to CCDC, 12 Union Road, Cambridge CB2 2EZ, UK; FAX: (+44) 1223 336033, or online via www.ccdc.cam.ac.uk/data_request/cif or by emailing data_request@ccdc.cam.ac.uk.

4. Conclusions and Perspectives

In conclusion, we have shown in this preliminary work that the Schiff base ligand *N*-naphthalidene-2-amino-5-chlorophenol (*nacpH*₂), in conjunction with the capping anion of 3,5-heptadione, is indeed capable of yielding new Dy^{III} complexes with rare structural motifs and interesting SMM properties. The reported [Dy₅(OH)₂(hpd)₃(nacp)₅(MeOH)₅] (**1**) cluster has no similarities with any of the previously reported {Dy^{III}_x} clusters bearing the structurally similar Schiff base ligands *saphH*₂ and *sacbH*₂ (Scheme 1). This emphasizes the bridging versatility of the dianion of *nacpH*₂ towards coordination with 4*f*-metal ions, and presages the creation of a rich, new library of cluster compounds with potentially exciting structural and magnetic properties.

Our future efforts are directed towards the chemical reactivity studies of *nacpH*₂ with 3*d*- and 4*f*-metal ions as a means of exploring the coordination capacity of this ligand in the presence of both transition metal ions and lanthanides. Another immediate target is the detailed study of the optical response of **1** to seek for any possible synergy between the SMM and photoluminescence properties. All these endeavors are in progress and the results will be reported in due course.

Supplementary Materials: The following are available online at <http://www.mdpi.com/2312-7481/4/4/48/s1>, Figure S1: Crystallographically established coordination modes of the ligands *nacp*²⁻ (top) and *hpd*⁻ (bottom) present in **1**. Figure S2: Field (*H*) dependence of the relaxation time (τ) of **1** measured at 2.0 K. The peak maximum corresponds to the optimum dc field. Figure S3: ¹H NMR spectrum of the ligand *nacpH*₂ in DMSO-*d*⁶. Figure S4: ¹³C NMR spectrum of the ligand *nacpH*₂ in DMSO-*d*⁶. Figure S5: Positive ESI-MS spectra of the ligand *nacpH*₂ in MeCN. The inset spectra show a zoomed picture of the experimental data (top) and the theoretical simulation of the isotope model of the protonated ion of *nacpH*₂ (bottom). Figure S6: Cole-Cole plots for **1** obtained using the ac susceptibility data at zero (top) and 200 Oe (bottom) applied dc fields. The solid lines are the best fit obtained from a generalized Debye model. Table S1: Selected interatomic distances (Å) and angles (°) for complex **1**. Table S2: Continuous shape measures (CShM) of the 8-coordinate Dy(1-5) coordination polyhedra in complex **1**. Table S3: Crystallographic data for complex $1 \cdot 3\text{MeOH} \cdot \text{CH}_2\text{Cl}_2$.

Author Contributions: D.I.A. and A.A.A. conducted the syntheses, crystallization, conventional characterization and interpretation of the structural and magnetic data for the organic ligand and the {Dy₅} cluster. D.S. collected single-crystal X-ray crystallographic data, solved the structure and performed the complete refinement. T.C.S. coordinated the research, contributed to the interpretation of the results and wrote the paper based on the reports of his collaborators. All the authors exchanged ideas and comments regarding the interpretation of the results and discussed upon the manuscript at all stages.

Funding: This research was funded by NSERC-DG, ERA and Brock University (Chancellor’s Chair for Research Excellence) to Th.C.S. This work was also supported by the National Natural Science Foundation of China (Grant Nos. 21822107 and 21571115 to D.S.).

Conflicts of Interest: The authors declare no conflict of interest.

References

1. Peng, J.-B.; Kong, X.-J.; Zhang, Q.-C.; Orendac, M.; Prokleska, J.; Ren, Y.-P.; Long, L.-S.; Zheng, Z.; Zheng, L.-S. Beauty, Symmetry, and Magnetocaloric Effect—Four-Shell Keplerates with 104 Lanthanide Atoms. *J. Am. Chem. Soc.* **2014**, *136*, 17938–17941. [[CrossRef](#)] [[PubMed](#)]
2. Bünzli, J.-C.G.; Eliseeva, S.V. Basics of Lanthanide Photophysics. In *Lanthanide Luminescence*; Springer Series on Fluorescence; Springer: Berlin/Heidelberg, Germany, 2010; pp. 1–45.
3. Tang, J.; Zhang, P. *Lanthanide Single Molecule Magnets*; Springer: Berlin/Heidelberg, Germany, 2015.
4. Gatteschi, D.; Sessoli, R.; Villain, J. *Molecular Nanomagnets*; Oxford University Press: Oxford, UK, 2006.
5. Layfield, R.A.; Murugesu, M. *Lanthanides and Actinides in Molecular Magnetism*; John Wiley & Sons: Hoboken, NJ, USA, 2015.
6. Bogani, L.; Wernsdorfer, W. Molecular Spintronics Using Single-Molecule Magnets. *Nat. Mater.* **2008**, *7*, 179–186. [[CrossRef](#)] [[PubMed](#)]
7. Sessoli, R.; Powell, A.K. Strategies towards Single Molecule Magnets Based on Lanthanide Ions. *Coord. Chem. Rev.* **2009**, *253*, 2328–2341. [[CrossRef](#)]
8. Zhang, P.; Guo, Y.-N.; Tang, J. Recent Advances in Dysprosium-based Single Molecule Magnets: Structural Overview and Synthetic Strategies. *Coord. Chem. Rev.* **2013**, *257*, 1728–1763. [[CrossRef](#)]
9. Rinehart, J.D.; Long, J.R. Exploiting Single-Ion Anisotropy in the Design of f-Element Single-Molecule Magnets. *Chem. Sci.* **2011**, *2*, 2078–2085. [[CrossRef](#)]
10. Mazarakioti, E.C.; Cunha-Silva, L.; Bekiari, V.; Escuer, A.; Stamatatos, T.C. New Structural Topologies in 4f-Metal Cluster Chemistry from Vertex-sharing Butterfly Units: {LnIII₇} Complexes Exhibiting Slow Magnetization Relaxation and Ligand-centred Emissions. *RSC Adv.* **2015**, *5*, 92534–92538. [[CrossRef](#)]
11. Mazarakioti, E.C.; Regier, J.; Cunha-Silva, L.; Wernsdorfer, W.; Pilkington, M.; Tang, J.; Stamatatos, T.C. Large Energy Barrier and Magnetization Hysteresis at 5 K for a Symmetric {Dy₂} Complex with Spherical Tricapped Trigonal Prismatic DyIII Ions. *Inorg. Chem.* **2017**, *56*, 3568–3578. [[CrossRef](#)] [[PubMed](#)]
12. Perlepe, P.S.; Cunha-Silva, L.; Gagnon, K.J.; Teat, S.J.; Lampropoulos, C.; Escuer, A.; Stamatatos, T.C. “Ligands-with-Benefits”: Naphthalene-Substituted Schiff Bases Yielding New NiII Metal Clusters with Ferromagnetic and Emissive Properties and Undergoing Exciting Transformations. *Inorg. Chem.* **2016**, *55*, 1270–1277. [[CrossRef](#)] [[PubMed](#)]
13. Habib, F.; Murugesu, M. Lessons Learned from Dinuclear Lanthanide Nano-magnets. *Chem. Soc. Rev.* **2013**, *42*, 3278–3288. [[CrossRef](#)] [[PubMed](#)]
14. Habib, F.; Brunet, G.; Vieru, V.; Korobkov, I.; Chibotaru, L.F.; Murugesu, M. Significant Enhancement of Energy Barriers in Dinuclear Dysprosium Single-Molecule Magnets through Electron-Withdrawing Effects. *J. Am. Chem. Soc.* **2013**, *135*, 13242–13245. [[CrossRef](#)] [[PubMed](#)]
15. Tian, H.; Zhao, L.; Lin, H.; Tang, J.; Li, G. Butterfly-Shaped Pentanuclear Dysprosium Single-Molecule Magnets. *Chem. Eur. J.* **2013**, *19*, 13235–13241. [[CrossRef](#)] [[PubMed](#)]
16. Biswas, S.; Das, S.; van Leusen, J.; Kögerler, P.; Chandrasekhar, V. Pentanuclear [2.2] Spirocyclic Lanthanide(III) Complexes: Slow Magnetic Relaxation of the DyIII Analogue. *Dalton Trans.* **2015**, *44*, 19282–19293. [[CrossRef](#)] [[PubMed](#)]
17. Yadav, M.; Mondal, A.; Mereacre, V.; Kumar Jana, S.; Powell, A.K.; Roesky, P.W. Tetranuclear and Pentanuclear Compounds of the Rare-Earth Metals: Synthesis and Magnetism. *Inorg. Chem.* **2015**, *54*, 7846–7856. [[CrossRef](#)] [[PubMed](#)]
18. Das, S.; Dey, A.; Kundu, S.; Biswas, S.; Suriya Narayanan, R.; Titos-Padilla, S.; Lorusso, G.; Evangelisti, M.; Colacio, E.; Chandrasekhar, V. Decanuclear Ln₁₀ Wheels and Vertex-Shared Spirocyclic Ln₅ Cores: Synthesis, Structure, SMM Behavior, and MCE Properties. *Chem. Eur. J.* **2015**, *21*, 16955–16967. [[CrossRef](#)] [[PubMed](#)]
19. Llunell, M.; Casanova, D.; Girera, J.; Alemany, P.; Alvarez, S. *SHAPE*, version 2.0; SHAPE: Barcelona, Spain, 2010.

20. Zabrodsky, H.; Peleg, S.; Avnir, D. Continuous Symmetry Measures. 2. Symmetry Groups and the Tetrahedron. *J. Am. Chem. Soc.* **1993**, *115*, 8278–8289. [[CrossRef](#)]
21. Cole, K.S.; Cole, R.H. Dispersion and Absorption in Dielectrics I. Alternating Current Characteristics. *J. Chem. Phys.* **1941**, *9*, 341–351. [[CrossRef](#)]
22. Demir, S.; Zadrozny, J.M.; Nippe, M.; Long, J.R. Exchange Coupling and Magnetic Blocking in Bipyrimidyl Radical-Bridged Divalent Lanthanide Complexes. *J. Am. Chem. Soc.* **2012**, *134*, 18546–18549. [[CrossRef](#)] [[PubMed](#)]
23. Woodruff, D.N.; Winpenny, R.E.P.; Layfield, R.A. Lanthanide Single-Molecule Magnets. *Chem. Rev.* **2013**, *113*, 5110–5148. [[CrossRef](#)] [[PubMed](#)]
24. Liddle, S.T.; Van Slageren, J. Improving f-Element Single Molecule Magnets. *Chem. Soc. Rev.* **2015**, *44*, 6655–6669. [[CrossRef](#)] [[PubMed](#)]
25. Habib, F.; Lin, P.-H.; Long, J.; Korobkov, I.; Wernsdorfer, W.; Murugesu, M. The Use of Magnetic Dilution to Elucidate the Slow Magnetic Relaxation Effects of a Dy₂ Single-Molecule Magnet. *J. Am. Chem. Soc.* **2011**, *133*, 8830–8833. [[CrossRef](#)] [[PubMed](#)]
26. Guo, Y.-N.; Xu, G.-F.; Guo, Y.; Tang, J. Relaxation Dynamics of Dysprosium(III) Single Molecule Magnets. *Dalton Trans.* **2011**, *40*, 9953–9963. [[CrossRef](#)] [[PubMed](#)]
27. Richardson, M.F.; Wagner, W.F.; Sands, D.E. Anhydrous and Hydrated Rare Earth Acetylacetonates and Their Infrared Spectra. *Inorg. Chem.* **1968**, *7*, 2495–2500. [[CrossRef](#)]
28. Bain, G.A.; Berry, J.F. Diamagnetic Corrections and Pascal's Constants. *J. Chem. Educ.* **2008**, *85*, 532–536. [[CrossRef](#)]
29. Palatinus, L.; Chapuis, G. SUPERFLIP—A Computer Program for the Solution of Crystal Structures by Charge Flipping in Arbitrary Dimensions. *J. Appl. Crystallogr.* **2007**, *40*, 786–790. [[CrossRef](#)]
30. Sheldrick, G.M. Crystal Structure Refinement with SHELXL. *Acta Crystallogr. C* **2015**, *71*, 3–8. [[CrossRef](#)] [[PubMed](#)]
31. Dolomanov, O.V.; Bourhis, L.J.; Gildea, R.J.; Howard, J.A.K.; Puschmann, H. OLEX2: A Complete Structure Solution, Refinement and Analysis Program. *J. Appl. Crystallogr.* **2009**, *42*, 339–341. [[CrossRef](#)]
32. Bradenburg, K.; Putz, H. *DIAMOND, Release 3.1f, Crystal Impact GbR*; DIAMOND: Bonn, Germany, 2008.



© 2018 by the authors. Licensee MDPI, Basel, Switzerland. This article is an open access article distributed under the terms and conditions of the Creative Commons Attribution (CC BY) license (<http://creativecommons.org/licenses/by/4.0/>).